

Analysis of discriminants for experimental 3-D SAR imagery of human targets

Brigitte Chan^{*a}, Pascale Sévigny^a, David D. J. DiFilippo^a

^aDefence Research & Development Canada, 3701 Carling Avenue, Ottawa, ON, Canada, K1A 0Z4

ABSTRACT

Development of a prototype 3-D through-wall synthetic aperture radar (SAR) system is currently underway at Defence Research & Development Canada. The intent is to map out building wall layouts and to detect targets of interest and their location behind walls such as humans, arms caches, and furniture. This situational awareness capability can be invaluable to the military working in an urban environment. Tools and algorithms are being developed to exploit the resulting 3-D imagery. Current work involves analyzing signatures of targets behind a wall and understanding the clutter and multipath signals in a room of interest. In this paper, a comprehensive study of 3-D human target signature metrics in free space is presented. The aim is to identify features for discrimination of the human target from other targets. Targets used in this investigation include a human standing, a human standing with arms stretched out, a chair, a table, and a metallic plate. Several features were investigated as potential discriminants and five which were identified as good candidates are presented in this paper. Based on this study, no single feature could be used to fully discriminate the human targets from all others. A combination of at least two different features is required to achieve this.

Keywords: through-wall, human target signature, L-band, SAR, detection, discriminants, segmentation

1. INTRODUCTION

The analysis of through-wall radar imagery is an emerging research area [1]. Many commercial products exist today to detect humans and other objects behind walls [2 - 8]. DRDC Ottawa has been investigating 3-D through wall synthetic aperture radar (SAR) imaging from an experimental L-band through-wall SAR prototype [9]. Tools and algorithms for 3-D visualization are being developed to exploit the resulting imagery. The intent is to provide situational awareness capability to the military working in an urban environment in the form of building wall layouts and target detection such as humans, arms caches, and furniture. In this paper, a comprehensive study of the characteristics of free-space target signatures is presented using 3-D SAR data from the through wall SAR prototype. The aim is to identify features for discrimination of the human target from other targets. Targets used in this investigation include humans in a standing position with arms resting at its side, humans standing with arms stretched out, a chair, and a table, all at 10m in range with reference to the truck-mounted radar system at closest approach, as well as a metallic plate at 5m in range. Photographs of the targets are presented in Figure 1.



Figure 1. Photographs of the targets: humans standing, humans standing arms stretched, table, chair, and metallic plate.

The experimental SAR radar testbed operates in the L-band. The side-looking radar is truck-mounted with data collected as the vehicle is driven along the SAR path parallel to the building of interest. The system operates over a 1.86 GHz bandwidth between 0.85 and 2.71 GHz. A LIDAR provides high resolution images of the exterior of a building, adding another layer of information to help with the interpretation of the SAR imagery. The azimuth direction is parallel to the SAR path while the range direction is perpendicular to it. Offline, following acquisition, the raw SAR data are pulse-compressed in range and then a backprojection algorithm is applied to form the SAR image [10].

Transmit and receive antenna elements of the SAR through-wall radar have a very broad beamwidth in azimuth up to 150 degrees. The radar operator can take advantage of the wide beamwidth and use a squinted SAR geometry which makes it possible to eliminate or minimize specular signal returns parallel to the SAR path, such as those due to a front wall while at the same time emphasizing features perpendicular to the SAR path, such as side walls. This is carried out by processing of the signal data to effectively illuminate and receive signals at an angle. Studying signatures of targets at varying squint angles can be used to investigate if they differ significantly with and without squint. SAR data were processed using three different parameter configurations: no squint, leading squint, and trailing squint.

In Section 2.0, signatures of the human, chair, table, and metallic plate are presented. In Section 3.0, discriminants for human target detection and future feature classification schemes are identified and analysis of the utility of the target signature discriminants is given. Conclusions and future research are presented in Section 4.0.

2. 3-D SAR TARGET SIGNATURES

All targets were manually detected. The corresponding pixel of maximum intensity (PMI), the highest intensity value of that target, was identified for each target. A look at signatures of the targets for all three squinting cases is presented in this section: a human target in two positions in Section 2.1, and a chair, a table, and a metallic plate in Section 2.2.

2.1 Human target signature in free space

In this section, the signature of a human target in free-space is examined for two different body positions. In the first case, the human is standing with arms at his side; in the second the human is standing with both arms stretched parallel to the ground. A top view of 3-D SAR data for the human target in both positions is displayed in Figure 2 for no squint, leading squint, and trailing squint, respectively.

Here, the location of the PMI azimuth and range coordinates changed slightly between the three cases – with a maximum variation of 20cm. This is above the azimuth and range resolutions and can be accounted for by considering the human physique and the geometry of the squint angle. In this case, squint SAR has the same effect as pointing the radar 35 degrees from boresight in azimuth. Consequently, more of the side of the human is illuminated than the front. Since it is believed that the radar backscatter from a human is primarily from the skin [11], it follows that the PMI is simply shifted from the front of the lower sternum to the side of the lower ribs, by at most 20cm in azimuth and 10cm in range. This is illustrated in Figure 3, where a contour line of the human target signature is drawn at 3dB below the maximum intensity, for the three squinted angle cases. The human target is approximately drawn with a dashed line as a reference.

For the human with arms stretched case, the location of the PMI in azimuth and range varies by 30cm in azimuth and 10cm in range. This can once again be accounted for by considering the human physique and the geometry of the squint angle. In the images, the torso and the extended arms of the human are readily discernible. For some unexplained reason, there seems to be a strong return to the left of the human. It gives the impression that the left arm is more dominant in the image than the right arm. This rather large feature seems to dominate at all levels of elevation indicating that it does not form part of the arms of the human. In fact, it might be masking the left arm and thus could also explain the wider than expected “wing span” of the human arms.

The difference in the human signature between the standing position and the arms stretched position is easily seen. The appearance of the arm feature in the arms stretched position is due to the corner created between the arms and the body. The difference in the human signature between no squint and squint is also seen. The signature for the human standing position for no squint is very similar to the signature for leading and trailing squint, with only a slight shift in the PMI azimuth coordinate. The signature of the human arms stretched position for no squint is different than the signature for leading and trailing squint, where returns of the extended arms are de-emphasized for leading and trailing squint than for no squint.

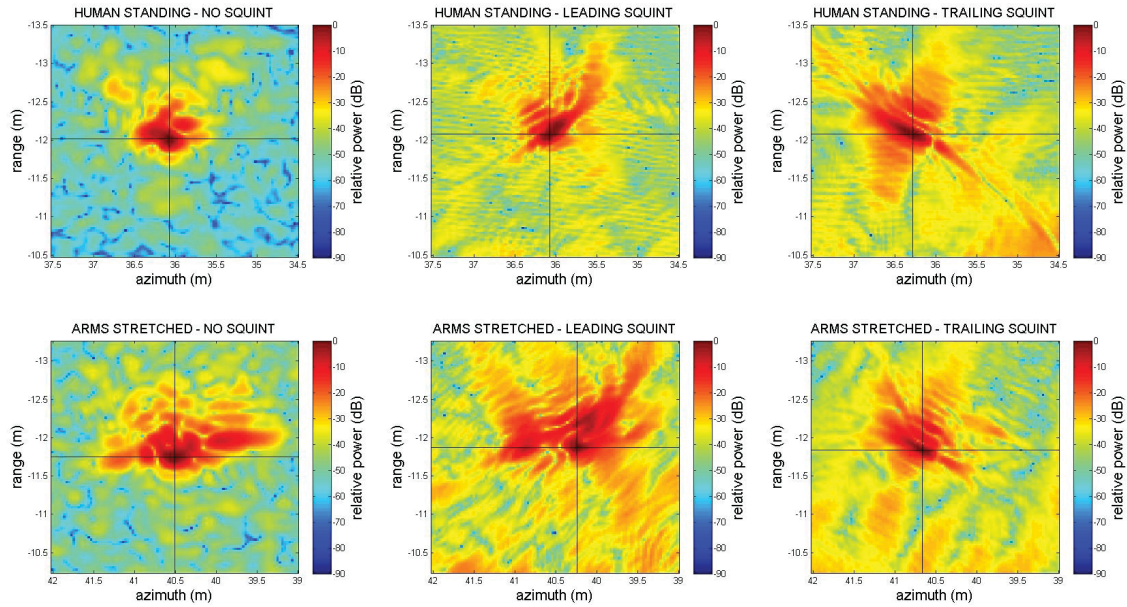


Figure 2. Top view 2-D slices at PMI elevation for human targets in two positions for no squint (left), leading squint (middle), and trailing squint (right): (top row) human standing and (bottom row) human standing with arms stretched.

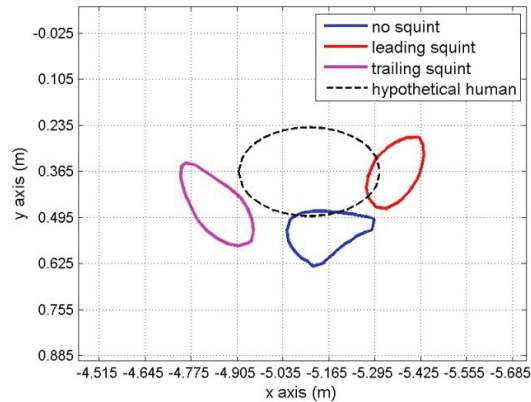


Figure 3. Experimental data displayed as 3dB contour, with grid spacing equal to the resolution.

2.2 Other 3-D SAR target signatures

In this section, the signature of a chair, a table, and a metallic plate in free-space is examined. A top view of 3-D SAR data for these three targets is displayed in Figure 4 for no squint, leading squint, and trailing squint, respectively.

The chair is composed of three materials: metal, cloth, and plastic. The chair legs which support the armrest and back, as well as the cushion support brackets underneath the chair, are metallic. The armrests are hard plastic. The seat cushion and chair back consist of a cloth material covering foam and corkboard. Five strong point returns are identifiable in the SAR images for the no squint case. Four of the strong returns correspond to each of the four metal legs of the chair. The strongest return corresponds to the corner created between the ground and each leg. The fifth return is the strongest and corresponds to a wide angled metallic corner formed at the junction between each half of the seat bracket. In the case of leading and trailing squint, only four strong target returns are observed, corresponding to each of the four metal chair legs. The fifth return seen in the no squint case does not appear in the image due to the scattering of the microwave signal away from the radar.

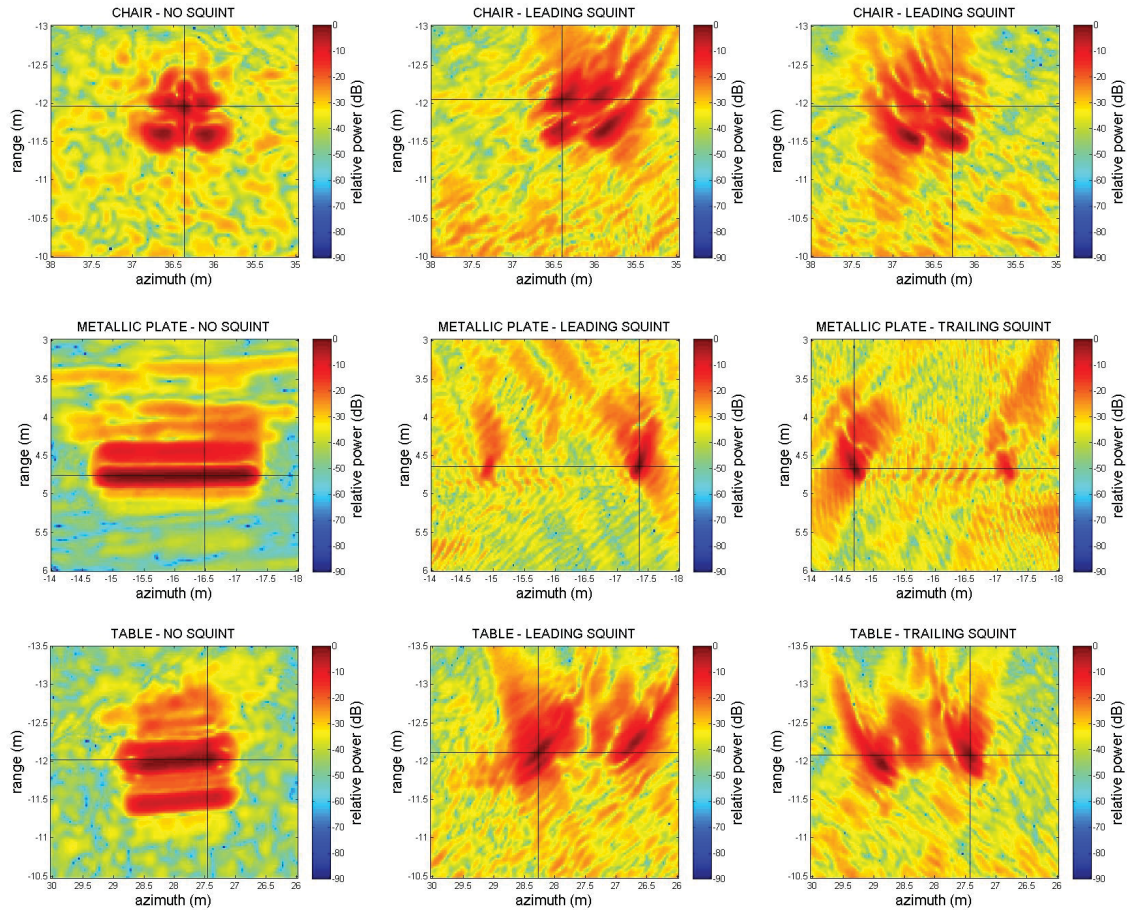


Figure 4. Top view 2-D slices at PMI elevation for no squint (left), leading squint (middle), and trailing squint (right) for a chair (top), a metallic plate (middle), and a table (bottom).

The metallic plate is supported by plastic tubes at each end. Two strong elongated returns are identifiable in the SAR images for the no squint case, centered at the same range at two distinct elevations. One return corresponds to the top edge of the metallic plate. The other strong return signal comes from the corner formed between the ground and the metallic plate. The width of the return is measured to be 2.0m in the azimuth direction. This is in close agreement with the physical length of the plate, differing by 20cm from that value. For the leading and trailing squint cases, the strong elongated return in azimuth seen for the no squint case does not appear. What remains is a strong return at the right and left edges of the metallic plate.

The table is composed of two materials: wood and metal. The table legs, crossbar plate, and the under table frame are metallic while the tabletop is wood. Only the metallic pieces are expected to have strong returns in the SAR imagery. Two strong elongated uniform returns are identifiable for the no squint case. The strong return at higher range corresponds to the crossbar and the strong return at lower range corresponds to the front of the support frame under the tabletop. Part of the contribution to the returns is also created by the corners formed between the table legs and feet. For both leading and trailing squint, the strong elongated returns seen for the no squint case do not appear. What remains are strong returns at the location of the crossbar. They are due to the corners created by the table foot and the ground, the table leg and the foot, and the metal crossbar and the metal leg.

Radar signatures in 3-D SAR imagery were studied for five different targets, namely, a standing human, a human with arms stretched, a chair, a metallic plate, and a table. In general, there was very close agreement between the measured physical dimensions of the targets and the values measured from the SAR imagery for the strong returns. The strong

returns in the SAR image from the non-human targets are mostly due to returns from metallic components and interactions between the metallic components and the ground.

The effects of a squinted SAR geometry on the target signatures were investigated by comparing these results to those for the no squint case. Returns from wide objects in the azimuth direction (parallel to the SAR path), such as those for the human arms, the chair cushion support bracket, the table crossbar and tabletop frame, and the top and bottom edges of the metallic plate, were significantly smaller than for no squint or non-existent. Features perpendicular to the SAR path that would otherwise not be seen in the no squint case became visible and dominant in the SAR images, including the sides of the human torso, the sides of the table legs and the side edges of the metallic plate. There was more similarity between the signatures of the human target for no squint and both leading and trailing squint compared to the differences observed for the other targets. This phenomenon could potentially serve as a feature used in discriminating the human target from all others.

Viewing of the SAR data as 2-D slices provides a qualitative means of discriminating between different target signatures. A more useful approach to discrimination would be to quantify these differences. In the next section, a look at different quantitative features as potential discriminants is investigated.

3. TARGET FEATURES

The differences in signatures for a number of targets were presented in Section 2. To the human eye, the differences between the signatures for the human, table, chair, and metallic plate are readily visible in the SAR images. In this section, potential quantitative features are investigated with the goal of finding discriminants for eventual detection and classification of human targets behind walls in the 3-D SAR images. For this analysis, all human targets in the data set are included. These include humans standing or with arms stretched who may be positioned behind other humans. As observed in the previous section, some targets, like the human target and the metallic plate, give rise to only one strong return while others, such as the chair and table, give rise to several strong returns or peaks. For targets having several strong returns, a decision must be made whether to evaluate each strong return separately, or to attempt to analyze them as a group when considering features. Both approaches have been investigated to see if discriminants can be identified.

Five different features are investigated: the PMI elevation coordinate feature in Section 3.1, the PMI intensity feature in Section 3.2, the 3dB width features in range and azimuth of the PMI profile in Section 3.3, the PMI intensity feature at varying range and azimuth in Section 3.4, and the number of resolution cells for 3-D volumes in Section 3.5. A summary and discussion of the results are presented in Section 3.6.

3.1 PMI elevation coordinate

The elevation of the PMI can differ between targets. Some targets produce very strong returns at the contact with the ground while for others, such returns are at various elevations above the ground. This feature is investigated as a potential discriminating factor for the human target.

Box plots of the PMI elevation coordinate data for each target were created and can be seen in Figure 5. A boxplot is a graphical representation of a distribution [4]. It displays differences between populations without making any assumptions of the underlying statistical distribution. For each box plot, the central mark in red represents the median of the data. The edges of the blue box represent the 25th and 75th percentiles at the bottom and at the top, respectively. Whiskers extend to the most extreme data points not considered as outliers. Where outliers exist, they are plotted individually as red stars. In order for a PMI elevation coordinate feature to be a good candidate for human target discrimination, no overlap between the human box plot and all others is desired.

All data, including those for no squint, leading squint, and trailing squint, are grouped together since the variation between the locations of the PMI elevation coordinate values is minimal. Results for all human targets whether standing or with arms stretched are used for the first box plot. Each individual strong return from the chair and table targets is included in the creation of the second and third box plots. Results for the metallic plate are used for the last box plot.

There is clearly a difference between PMI elevation coordinate of the human target and the table and chair targets. Whereas this value is 1.0m above ground on average for the human target, the values for the table and chair are much closer to the level of the ground. There is no overlap in any of the elevation values between the human target and the chair and table targets. The metallic plate has the same median location of the PMI elevation coordinate as the human target and cannot be discriminated from the human target with this feature.

The PMI elevation coordinate feature is a great candidate for discriminating the human target from other targets; however, it cannot be used to discriminate between them all. Other discriminants are needed to fully and robustly discriminate the human target from all others. Furthermore, the orientation and position of the human target is an important consideration. Close agreement between the locations of the PMI elevation coordinate is observed for both the standing human and the human with arms stretched. What still needs to be investigated is a human target in various other poses, such as seated and kneeling. The PMI elevation coordinate is sure to be lower in those circumstances which would make this feature ineffective for human target discrimination for a human in positions closer to the ground.

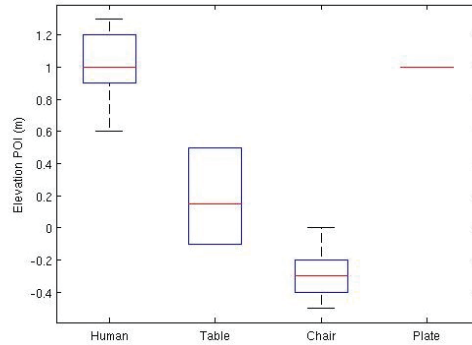


Figure 5. Box plots of PMI elevation coordinate for human, table, chair, and metallic plate targets.

3.2 PMI intensity

The peak intensity value at the PMI is considered as a feature for the no squint, leading squint, and trailing squint cases. Box plots of the peak intensity value at the PMI for each target are presented in Figure 6 for no squint, leading squint, and trailing squint, respectively.

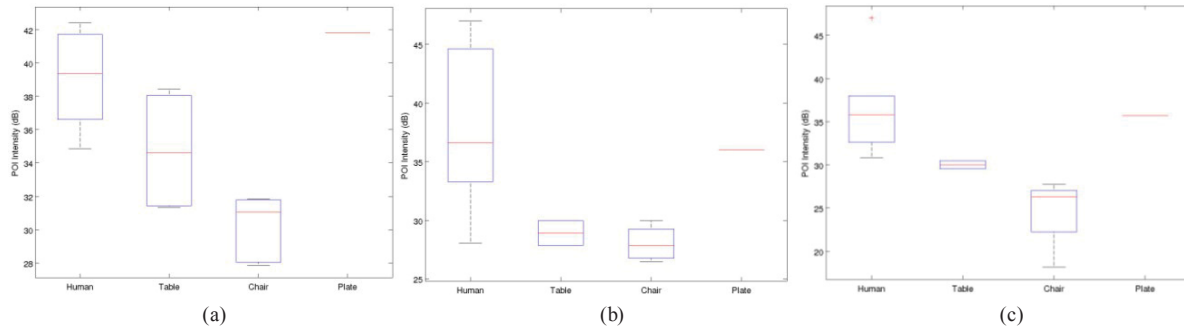


Figure 6. Box plots of PMI intensities of targets for (a) no squint case, (b) leading squint, and (c) trailing squint.

As seen in Figure 6, there is a discernible difference in peak intensity values between the target types although some overlap exists. The median PMI intensity values of the chair and table are all below the median PMI intensity values of the human target in all instances. For the no squint and the trailing squint cases, the chair can be completely discriminated from the human target as no overlap exists. Although the median PMI intensity of the table is lower than that of the human, overlap still occurs, especially for the no squint case. The overlap is very minimal for the leading and trailing squint cases. The PMI intensity values for the metallic plate are closest to the PMI intensity values for the human target although on the higher end when considering the no squint case. More exemplars of each target type are required to determine the true statistical nature of the data before discrimination can be achieved with this feature.

The PMI intensity feature is a good candidate for discriminating the human target from other targets; however, again, it cannot be used to discriminate fully. Other discriminants are needed to fully and robustly discriminate the human target from all others.

3.3 3dB width

The 3dB width in each of the range and azimuth directions of each target is considered as a feature. Unlike the 3dB width of a point target, where it is defined as radar resolution, the 3dB width of the different targets under consideration is a measure of the extent of the strong return.

Box plots of the 3dB width in azimuth for each target were created for the no squint, leading squint, and trailing squint cases. The 3dB width in azimuth is shown in Figure 7(a) while the 3dB width in range is shown in Figure 7(b). The lettering of the labels on the x-axis has the format *XY*, where *X* is the first letter of the target type (H for human, T for table, C for chair, and P for metallic plate) and *YY* provides the initials for the squint geometry used (NS for no squint, LS for leading squint, and TS for trailing squint).

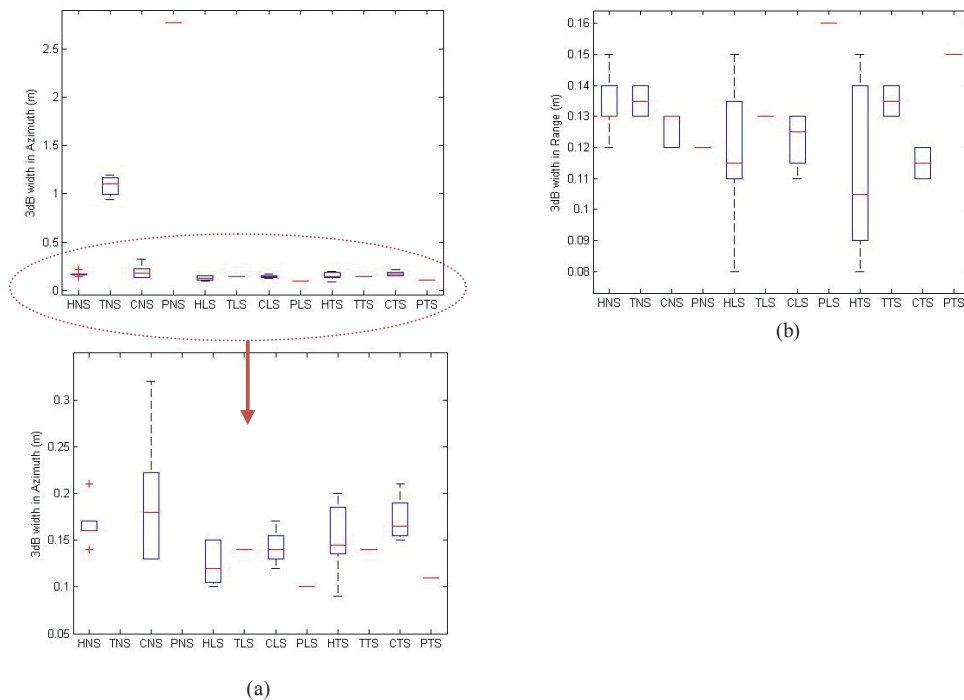


Figure 7. Box plots of 3dB width in (a) azimuth and (b) range of human (H), table (T), chair (C), and metallic plate (P) targets for no squint (NS), leading squint (LS), and trailing squint (TS).

Two features stand out in Figure 7(a). The values for the table and metallic plate targets for the no squint condition are well above those of all other targets by a factor varying from 10 to almost 30 in the azimuth direction. A closer look at the box plots of Figure 7(a), without these two high 3dB width values can be seen in the lower image. There appears to be a high level of overlap between all other targets along the azimuth dimension, where the median varies very little (between 0.10dB and 0.18dB).

There appears to be significant overlap between all targets for the range 3dB widths in Figure 7(b). As seen for the azimuth 3dB width, the median varies very little again (between 0.11dB and 0.16dB). Even though the values for the metallic plate appear to be above that for the human in the leading and trailing squint cases, the difference is not great enough to confidently use the 3dB width in range for discrimination. It can still remain a consideration if other objects with large 3dB widths along the range direction are considered as targets in the future.

Using the average 3dB width in the azimuth direction for the no squint case would be a practical choice to consider in future human target discrimination applications even though it also cannot be used to fully discriminate the human target from all other targets. The average 3dB width in the range direction could still remain a consideration as a way to discriminate the human target from objects having large 3dB widths in that direction.

3.4 Maximum intensity profile

Variations in the maximum intensity in range in the azimuth direction for increasing distances from the PMI have been examined. Similarly, variations in the maximum intensity in azimuth in the range direction for increasing distances from the PMI have also been examined. These two dimensions were chosen due to their higher spatial resolution. To create the profile of maximum intensities in the azimuth direction, the maximum intensity at the location of the PMI is found. The maximum intensity in range at one azimuth grid point further from the location of the PMI is then determined, as is shown pictorially in Figure 8. This process of finding the maximum intensity at the next azimuth grid point continues until a maximum intensity profile in the azimuth direction is created. To create the maximum intensity profile in the range direction, the same process as that described for the maximum intensity profile in the azimuth direction is used to find the maximum intensities at increasing range distances from the location of the PMI. The elevation remains constant throughout at the value for the PMI.

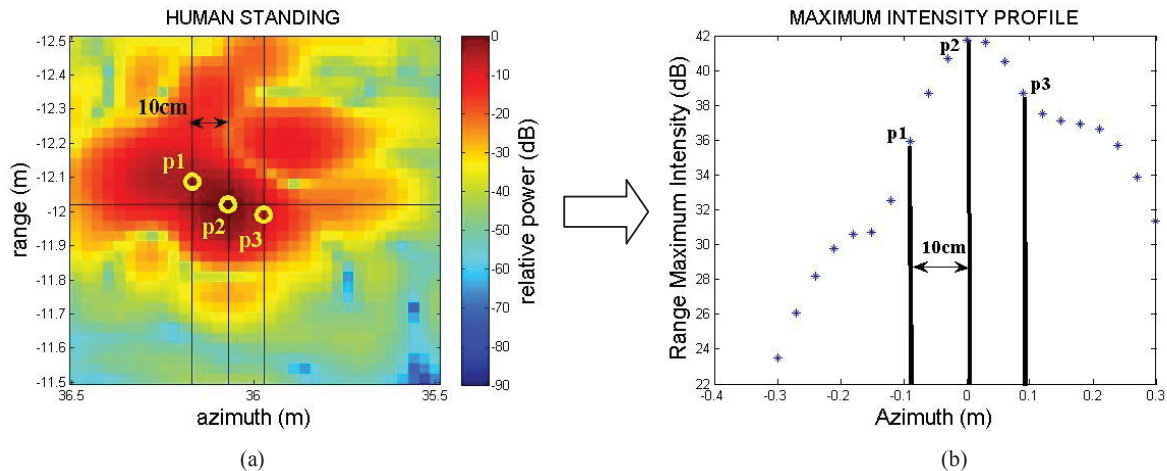


Figure 8. Pictorial representation of how the maximum intensity profile in range at varying azimuth positions is created for a target; showing here three pixel values 10cm apart, whereas 21 pixel values 3cm apart are extracted to create the full maximum intensity profile. (a) Top view of human signature showing pixel locations where maximum intensity values p1, p2, and p3 are extracted to create the maximum intensity profiles; (b) Maximum intensity profile created, highlighting the three maximum intensity values extracted from (a).

For this study, the distance from the PMI is arbitrarily chosen to vary from 30cm in front of to 30cm behind the PMI in the azimuth direction and similarly from 30cm to the left to 30cm to the right of the PMI in the range direction. The assumption is that at increasing distances from the PMI, the maximum intensity decreases at different rates or in different patterns for each of the targets which can make it possible to discriminate one target from all others.

The range and azimuth maximum intensity at varying range and azimuth locations, respectively, were determined for all targets including all humans (H1 to H5 representing standing human and H6 to H8 representing human arms stretched), each bright spot for each end of the table (T1 to T4), each bright spot of the chair (C1 to C5), and the metallic plate (P) for the no squint case.

To quantify the difference between the range maximum intensity variations in the azimuth direction, a correlation matrix was obtained for all pairs of the profile curves. A color visual representation is given in Figure 9(a). For this feature to be a good candidate for discrimination of the human target from all others, a strong correlation of 0.85 and above is desired between each pair of the profiles for the human, and a weaker correlation of less than 0.6 is desired between each pair for the human and all others.

High correlation is observed between each pair of curves for the human targets. This is desirable. High correlation is also observed between the human target and metallic plate, and between the human targets and the chair peaks C1 and C5. This is not desirable; however, low correlation exists between the human targets and all four table peaks, and between the human targets and three chair peaks C2, C3, and C4, which is again desirable. Although the human target cannot be

discriminated from the metallic plate using this metric, it can strongly be discriminated from the chair and table, making this feature a strong candidate for future discrimination of human targets from other targets.

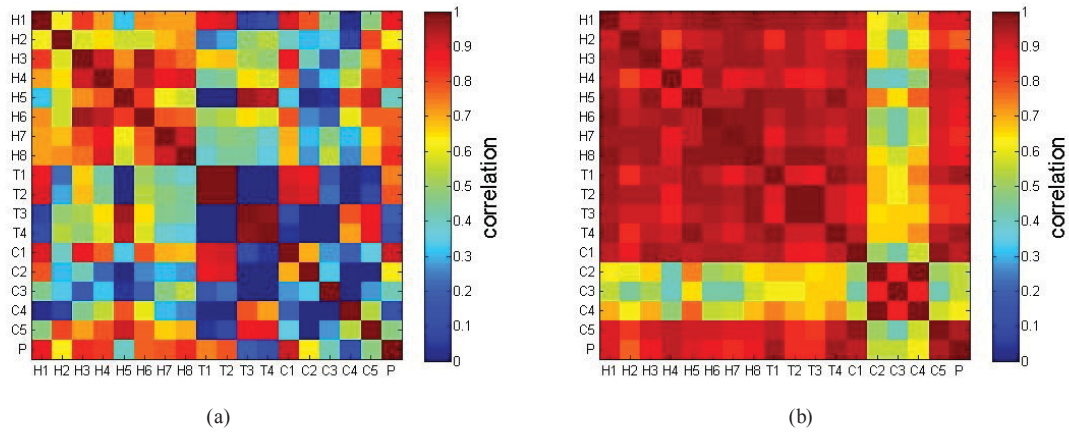


Figure 9. Correlation matrix of maximum intensity in (a) range at varying azimuth positions for all targets and (b) azimuth at varying range positions for all targets.

To quantify the difference between the azimuth maximum intensity variations in the range direction, a correlation matrix was obtained for all pairs of the profile curves. A color visual representation is given in Figure 9(b). Very high correlation is observed between each pair of curves for the human targets. Very high correlation is also seen between the human target curves and those for the peaks of the table and the metallic plate. This is not desirable for discrimination of the human target from the others. There is, however, very low correlation between the human target and the three peaks of the chair C2, C3, and C4, which is desirable. Considering the high level of similarity between each curve except for the three chair peaks C2, C3, and C4, this correlation matrix result is expected. Although the human target cannot be discriminated from the table and metallic plate using this metric, it can strongly be discriminated from the chair, making this feature a strong candidate for future discrimination of human targets.

The same process as above was conducted for the azimuth and range 3dB width profiles in the range and azimuth directions, respectively (not shown here). The azimuth and range 3dB width profiles in the range and azimuth directions, respectively, do not seem effective for discriminating the human target from other targets. Although some correlation exists for the azimuth 3dB width profiles between any of the human targets and between any human target and all others, particularly for the human arms stretched position, the correlation value is not as high as desired. For the range 3dB width profiles, very little correlation exists. Consequently, using this feature for complete discrimination between the human targets and all others is not recommended.

3.5 Number of resolution cells for 3-D volumes

A different perspective can be gained from viewing 3-D volumes of the SAR data instead of 2-D slices of the 3-D data. The PMI can be used as a seed point for a seeded region growing algorithm [13], where a given connected voxel is retained in the segmented volume if its value is greater than a fixed threshold (in dB) below the PMI value. Increasing the dB threshold used to view the image was investigated to see at what value other features of the target signatures, if any, become apparent in the 3-D volumes. A good metric for the 3-D volume analysis is the number of resolution cells the cubes occupy for each target volume. For consistency in comparison between each target, the same threshold must be used. A threshold of 24dB was chosen as it was the lowest threshold value necessary in order that all target features be visible. The volumes produced are shown in Figure 10. The number of resolution cells in azimuth, range, and elevation are presented in Table 1 for all five types of targets.

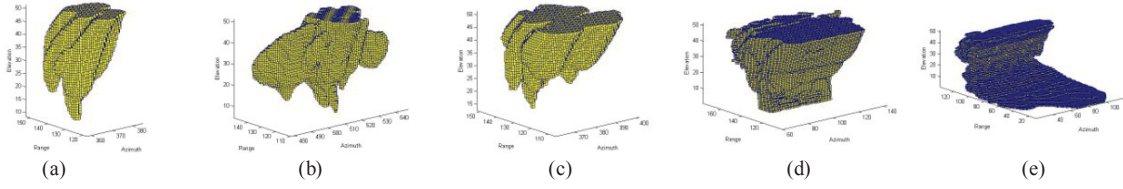


Figure 10. 3-D volumes at 24dB threshold for (a) human standing, (b) human arms stretched, (c) chair, (d) table, and (e) metallic plate.

Table 1. Number of resolution cells for 3-D volumes at 24dB threshold.

	azimuth	range	elevation
Human standing	9	12	6
Human arms stretched	23	13	6
Chair	14	15	6
Table	28	25	6
Plate	33	43	6

At a threshold of 24dB, there is enough difference in the numbers of azimuth resolution cells to be able to strongly discriminate the human standing target from the human arms stretched, table, and metallic plate targets. There is also enough difference in the number of range resolution cells to be able to discriminate the human standing and human arms stretched targets from the table and metallic plate. The difference in the numbers of resolution cells in the azimuth and range directions between the chair and the human standing target is only 2 to 5 cells. The number of resolution cells in elevation is similar for all cases. The number of resolution cells in azimuth feature does not appear to be a good candidate because of the high value of azimuth resolution cells for the human arms stretched target compared to that for the human standing target, making discrimination of all human targets from the others impossible for this case. Perhaps the unexplained strong return to the left of the human that dominates in the azimuth direction is skewing the results. More investigation is required to determine the true number of azimuth resolution cells for the human arms stretched target. It is concluded that the number of resolution cells in range feature would be a good candidate for the discrimination of the human target from the other targets but more investigation is required to conclude whether the number of resolution cells in azimuth feature would be a good candidate or not.

3.6 Summary and discussion of results

Five different approaches were introduced and analyzed for their capability to discriminate human targets from others in free space. A table summarizing the results of the analysis is presented in Table 2 indicating which approaches produced a strong candidate for discrimination, a candidate for discrimination with potential, and a poor candidate for discrimination. Although each approach showed potential for discriminating the human target from other targets, not one feature could be used to fully discriminate between all targets. Combining several features could perform this task. For example, the PMI elevation coordinate and the 3dB width features could provide a means to fully discriminate the human target from all others presented in this study. Results presented in this section are preliminary. A larger set of different target types, especially those typically found in buildings of interest, is necessary. As well, the limited number of exemplars of each of the targets used in this study is not sufficient to make conclusive remarks. Use of a larger set of exemplars of the same type of target, in the same position and at different orientations and positions, would give more confidence in the values obtained for the different features. This would be a more robust analysis and would be a prudent approach to eliminating anomalies observed in the data. For example, if multiple subjects and objects of a given type could be used, a more accurate box plot can be generated, perhaps with smaller variations between the lowest and highest values in the data. This would provide a more realistic metric to investigate if this feature could be used to discriminate the human target from the table.

4. CONCLUSIONS AND FUTURE RESEARCH EFFORTS

In this paper, a comprehensive study of the characteristics of free-space target signatures was presented using 3-D SAR data. An analysis of different target signatures was provided. Several features were investigated as potential discriminants and five which were identified as good candidates were presented. All of the discriminants measured or calculated in this paper have relied heavily on the PMI and the PMI intensity. The PMI is not only important for the





extraction of the discriminants, but also for forming the seed to many available segmentation algorithms. Five different discrimination approaches were identified as showing great potential of features that could be used to discriminate the human target from all others: PMI elevation coordinate, PMI intensity, 3dB width in azimuth of the no squint case, and the number of resolution cells in range. Based on the free-space scenario and the different targets in this study, no single feature could be used to fully discriminate the human targets from all others. A combination of at least two different features is required to achieve this.

This study will be continued to search for more features and will be enlarged to include more targets in different orientations as well as more exemplars of the human target in various positions in order to create a robust strategy for detection and classification of human targets. The research will be expanded to include an investigation of how the signatures of targets vary as they are moved behind different types of walls. Furthermore, a thorough understanding of the clutter and multipath present behind walls are required if the signature of the human target is to be extracted and discriminated from these noise sources. Eventually, efforts will be made to choose the most effective classifier for the discrimination of human targets from all others.

Table 2. Summary of results for discriminants.

	No Squint			Leading Squint			Trailing Squint		
	Chair	Table	Plate	Chair	Table	Plate	Chair	Table	Plate
PMI elevation	Green	Green	Red	Green	Green	Red	Green	Green	Red
PMI intensity	Green	Red	Yellow	Yellow	Yellow	Red	Green	Yellow	Red
3dB width in azimuth	Red	Green	Green	Red	Red	Yellow	Red	Red	Yellow
3dB width in range	Red	Red	Red	Red	Red	Yellow	Red	Red	Red
Max. intensity in azimuth	Green	Red	Red	Grey	Grey	Grey	Grey	Grey	Grey
Max. intensity in range	Red	Red	Red	Grey	Grey	Grey	Grey	Grey	Grey
Number of azimuth cells	Yellow	Green	Green	Grey	Grey	Grey	Grey	Grey	Grey
Number of range cells	Red	Green	Green	Grey	Grey	Grey	Grey	Grey	Grey
Number of elevation cells	Red	Red	Red	Grey	Grey	Grey	Grey	Grey	Grey

Legend:

	Strong candidate for discrimination
	Candidate for discrimination with potential
	Not a good candidate for discrimination
	Analysis not conducted

REFERENCES

- [1] Amin, Moeness G, [Through-the-wall RADAR imaging], CRC Press, Florida ((2011).
- [2] Prism 200: Through Wall Radar, Cambridge Consultants, June 11, 2014, <http://www.cambridgeconsultants.com/projects/prism-200-through-wall-radar>
- [3] Xaver Products, Camero, June 11, 2014, <http://www.camero-tech.com/products.php>
- [4] EMMDAR (Electro-Magnetic Motion detection And Ranging), L3 CyTerra, June 11, 2014, <http://www.cytterra.com/products/emmdar.htm>
- [5] Range-R, L3 CyTerra, June 11, 2014, <http://www.cytterra.com/products/ranger.htm>
- [6] ASTIR: Standoff Through-Wall Imaging Radar, Akela, June 11, 2014, <http://www.akelainc.com/products/astir>
- [7] CPR-4, Cinside, June 11, 2014, <http://cinside.se/e/products/cinside-cpr4>
- [8] O-PEN Radar, SRC, June 11, 2014, <http://www.srcinc.com/what-we-do/radar-and-sensors/o-pen-radar.html>

- [9] Sévigny, P., DiFilippo, D.J., Laneve, T., Chan, B., Fournier, J., Roy, S., Ricard, B., and Maheux, J., "Concept of operation and preliminary experimental results for the DRDC through-wall SAR system," Proc. Of SPIE, 7669, 766907-766907-11 (2010).
- [10] Soumekh, M., [Synthetic aperture radar signal processing], John Wiley and Sons, 1999.
- [11] Dogaru, T., Nguyen, L., and Le, C., "Computer models of the human body signature for sensing through the wall radar applications," AL-TR-4290, Army research Lab (2007).
- [12] McGill, R., Tukey, J. W., and Larsen, W.A. "Variations of Boxplots," The American Statistician, 32(1), 12-16 (1978).
- [13] Adams, R., Bischof, L. "Seeded region growing," IEEE Transactions of Pattern Analysis and Machine Intelligence, 16(6), 641-647 (1994).